HHS Public Access

Author manuscript

Nat Cell Biol. Author manuscript; available in PMC 2015 October 01.

Published in final edited form as:

Nat Cell Biol. 2015 April ; 17(4): 386–396. doi:10.1038/ncb3139.

The suture provides a niche for mesenchymal stem cells of craniofacial bones

Hu Zhao, **Jifan Feng**, **Thach-Vu Ho**, **Weston Grimes**, **Mark Urata**, and **Yang Chai***

Center for Craniofacial Molecular Biology, Ostrow School of Dentistry, University of Southern California, 2250 Alcazar Street, CSA 103, Los Angeles, CA 90033

Abstract

Bone tissue undergoes constant turnover supported by stem cells. Recent studies showed that perivascular mesenchymal stem cells (MSCs) contribute to the turnover of long bones. Craniofacial bones are flat bones derived from a different embryonic origin than the long bones. The identity and regulating niche for craniofacial bone MSCs remain unknown. Here, we identify *Gli1*+ cells within the suture mesenchyme as the major MSC population for craniofacial bones. They are not associated with vasculature, give rise to all craniofacial bones in the adult and are activated during injury repair. *Gli1*+ cells are typical MSCs *in vitro*. Ablation of *Gli1*+ cells leads to craniosynostosis and arrest of skull growth, indicating these cells are an indispensible stem cell population. *Twist1*$^{+/-}$ mice with craniosynostosis show reduced *Gli1*+ MSCs in sutures, suggesting that craniosynostosis may result from diminished suture stem cells. Our study indicates that craniofacial sutures provide a unique niche for MSCs for craniofacial bone homeostasis and repair.

Introduction

Craniofacial bones differ from the long bones. They are flat bones formed mainly through intramembranous rather than endochondral ossification and develop from embryological origins distinct from those of the long bones[1-3]. Perivascular mesenchymal stem cells (MSCs) have been identified in the bone marrow of the long bones and support their turnover and injury repair[4-7]. Craniofacial bones contain little bone marrow space and are sheathed by periosteum and endosteum or dura[8, 9]. Although the question of whether there is a specific stem cell population in adult craniofacial bones has remained unanswered, it was generally assumed that these flat bones share the same turnover and injury repair mechanisms as long bones. It has been proposed that the periosteum contains progenitors that support craniofacial bone repair[10-13].

*Corresponding author Correspondence to: Yang Chai <ychai@usc.edu>.

Contributions

H.Z. and Y.C. designed the study. H.Z. carried out most of the experiments and analyzed the data. J.F. participated in the suture cell culture experiments. T.H. and W.G. participated in the microCT analysis. M.U. provided comments. H.Z. and Y.C. co-wrote the paper. Y.C. supervised the research.

Competing financial interests

The authors declare no competing financial interests

The joints between craniofacial bones are known as sutures and are composed of two osteogenic fronts with suture mesenchyme between them (Supplementary Figure 1). Most sutures in mice remain patent throughout the animal's lifetime. In humans, cranial sutures normally fuse between 20 and 30 years of age and facial sutures fuse after 50 years of age[14, 15].

Craniosynostosis is a common congenital disorder characterized by premature cranial suture fusion, which may lead to severe outcomes including increased intracranial pressure, craniofacial dysmorphism, disrupted neurodevelopment, and mental retardation. Craniosynostosis is generally considered a developmental disorder resulting from a disrupted balance of cellular proliferation, differentiation and apoptosis within the suture[15-19]. Surgical removal of the affected suture followed by re-shaping of the calvarial bones remains the only treatment available for craniosynostosis patients[20-22]. Although the purpose of the surgery is to form artificial suture-like space between the calvarial bones to allow for brain expansion, the natural suture tissue is treated as surgical waste and routinely discarded during the procedure[23-25].

In our current study, using mouse craniofacial bones as a model, we identified *Gli1*+ cells within the suture mesenchyme as the major stem cell population for adult craniofacial bones. They give rise to the periosteum and dura. They are typical MSCs *in vitro* but are not associated with vasculature and are regulated by IHH secreted from the committed osteogenic progenitors. Ablation of *Gli1*+ cells in the adult mouse leads to craniosynostosis, skull growth arrest and osteoporosis. The Gli1+ cell population was diminished in craniosynostosis model *Twist1* $^{+/-}$ mutant mice, which suggests that compromised stem cells might be the cause of craniosynostosis. Our finding indicates that a different niche regulates the stem cells of craniofacial bones than that of long bones. Craniosynostosis, a severe congenital disease, might be caused by stem cell population defects.

Results

Gli1+ cells are specifically distributed in the suture mesenchyme of adult craniofacial bones

We hypothesized that *Gli1*+ cells are MSCs for craniofacial bones, as they are for the incisor mesenchyme[26]. First, we investigated the expression of *Gli1* in mouse calvarial bones. At postnatal day 0 (P0), *Gli1*+ cells are detectable throughout the entire periosteum, dura and suture mesenchyme, but not in the fontanelles or osteocytes (Figure 1a, g). A similar distribution pattern was detectable at P7 and P14 (Figure 1b-c, h-i). Between P21 and 1 month postnatally, *Gli1*+ cells are gradually restricted to the suture region (Figure 1d-e). At one month of age, *Gli1*+ cells are only detectable within the suture mesenchyme, mostly in the mid-suture region, but are absent from the periosteum, dura and osteocytes (Figure 1j-l). Such a suture-specific pattern was also detectable in mice at three months of age and older (Figure 1f).

We next investigated the *Gli1*+ cell distribution pattern in other craniofacial sutures. In *Gli1-LacZ* mice at one month of age, we detected *Gli1*+ cells in the mesenchyme of most craniofacial sutures, including the coronal (Figure 1m), interpalatal (Figure 1n),

presphenoid-palatal (Figure 1o), maxilla-palatal (Figure 1p), lambdoid (Supplementary Figure 2a), interparietal-occipital (Supplementary Figure 2b), parietal-squamous (Supplementary Figure 2c), maxilla-zygomatic (Supplementary Figure 2d), squamous-zygomatic (Supplementary Figure 2e), maxilla-premaxilla (Supplementary Figure 2f), frontal-maxilla (Supplementary Figure 2g), frontal-squamous (Supplementary Figure 2h), frontal-premaxilla (Supplementary Figure 2i), nasal-frontal (Supplementary Figure 2j), intermaxilla (Supplementary Figure 2k), basosphenoid-squamous (Supplementary Figure 2l) and basosphenoid-frontal (Supplementary Figure 2m) sutures. *Gli1+* cells are mainly present in the mid-suture mesenchyme and are absent from the periosteum, dura and bones abutting the sutures. Interestingly, *Gli1+* cells are not detectable in the posterior frontal suture mesenchyme at either P8 or P30. The posterior frontal suture is the only suture in the mouse that fuses around two weeks after birth[27-29].

Craniofacial bones contain little bone marrow space compared to long bones. *Gli1+* cells are also detectable on the inner surface of some bone marrow spaces (Supplementary Figure 4a). The number of these bone marrow *Gli1+* cells differs by location, but only comprises a minor population in craniofacial bones (Supplementary Figure 4b).

To investigate the differentiation status of suture *Gli1+* cells, we evaluated the expression of various osteogenic differentiation markers in the calvarial bones of one-month-old mice. All the markers we tested, including *ALPase, Sp7, Runx2* and *osteocalcin*, are strongly expressed in the periosteum and the dura, but are absent from the majority of the suture mesenchyme (Figure 1q-t). Within the suture, *Sp7* and *Runx2* are expressed in a few cells within the osteogenic fronts, which are thin layers of cells immediately lining the bony surface (Figure 1r', t'). Co-staining indicates *Gli1+* cells are located near, but not within, the osteogenic fronts (Supplementary Figure 2n)

Gli1+ cells in the suture mesenchyme give rise to osteogenic fronts, periosteum and dura

To test whether *Gli1+* cells in the suture mesenchyme are stem cells, we performed lineage tracing analysis. *Gli1-Cre^{ERT2};R26ZsGreen^{flox}* or *Gli1-Cre^{ERT2};R26Tdtomato^{flox}* mice (*Gli1-CE*) were induced with tamoxifen at 1 month of age. Five days after induction, fluorescently labeled cells were detectable exclusively in the mid-suture mesenchyme of the calvaria (Figure 2a) and other craniofacial bones (Figure 2e; Supplementary Figure 3a-m), faithfully reproducing the *Gli1+* cell distribution pattern. No signal was detectable in the osteogenic fronts (Supplementary Figure 3n), periosteum, dura or osteocytes of craniofacial bones. One month later, we detected fluorescently labeled cells in the entire suture mesenchyme including the osteogenic fronts (Supplementary Figure 3n', o'), part of the periosteum, dura and a few osteocytes next to the osteogenic fronts of calvarial bones (Figure 2b). Examination of other craniofacial sutures including the sutures in the basal skull region and facial region indicated that significant numbers of cells in the periosteum and bones were already strongly labeled with fluorescence one month after induction (Supplementary Figure 3a'-m'). The presence of *Gli1+* cells in these structures can be attributed to both the postnatal growth of the skull vault and the postnatal turnover of craniofacial bones. The turnover rates of different craniofacial bones vary significantly and calvarial bones turn over much slower than other craniofacial bones.

Two months after induction, the entire suture mesenchyme, periosteum and dura as well as parts of the calvarial bones were strongly labeled (Figure 2c). Most of the labeled calvarial osteocytes were located either next to the suture or peripherally, indicating that new bone deposits mostly at the osteogenic front region and external surface of the calvarial bones. Eight months after induction, the entire calvaria including the suture mesenchyme, periosteum, dura and almost every osteocyte were strongly labeled, suggesting a complete turnover of calvarial bone within this time period (Figure 2d).

Gli1+ cells in the bone marrow also give rise to osteocytes immediately surrounding the bone marrow space, but not to blood cells (Supplementary Figure 4c-d). Their contribution to craniofacial bones is limited due to the small percentage of Gli1+ cells in the bone marrow space.

Gli1+ cells contribute to injury repair and transplant growth

Gli1+ cells in the suture mesenchyme normally do not undergo active division. However, within 24 hours after an injury, they can be rapidly activated into proliferation (Figure 3a-b). To investigate the contribution of *Gli1*+ cells to injury repair, we induced *Gli1-CE* mice with tamoxifen at one month of age and made an injury to the calvarial bone. Two weeks after injury, most of the cells within the injured region were strongly labeled, indicating their derivation from *Gli1*+ cells (Figure 3c). One month after injury, the periosteum, dura and many osteocytes in the repair region were strongly labeled, indicating *Gli1*+ cells contribute to post-injury repair of the calvarial bone (Figure 3d).

Previously, it was proposed that progenitor cells supporting craniofacial bone repair mainly reside in the periosteum. Our lineage tracing analysis indicated that, instead, the suture mesenchyme gives rise to the periosteum and dura during natural turnover. To confirm this relationship, we induced *Gli1-CE* mice at one month of age. After removing the periosteum and dura, we transplanted a piece of calvarial bone containing the sagittal suture into nude mice.

Only the suture mesenchyme was labeled in samples collected 72 hours after transplantation (Figure 3e). One week after transplantation, newly generated, fluorescently labeled periosteum and dura were detectable on the surfaces of the transplants (Figure 3f). One month after transplantation, the suture transplants merged with the host bone. A significant number of cells within the periosteum, dura and bone (osteocytes) of the transplant were strongly labeled, indicating their derivation from the *Gli1*+ cells within the suture mesenchyme (Figure 3g). Calvarial bones not containing any suture taken from the same donor mice were also transplanted as controls (Figure 3h). Although *Gli1*+ cells in the bone marrow space survived one month after transplantation, they failed to generate new periosteum, dura or osteocytes. Therefore, bone marrow *Gli1*+ cells are either incapable or insufficient to support efficient repair or regeneration.

To evaluate the regeneration ability of suture tissue and specifically to compare it with the periosteum, we transplanted calvarial bones with or without suture from *CMV-EGFP* mice of one month of age into nude mice. The suture transplants grew rapidly and doubled their surface area within one month, whereas the control calvarial bone transplants without

sutures failed to grow even though they contained intact periosteum and dura (Figure 3i-j). This result indicates the suture tissue possesses regenerative capacity but periosteum and dura do not, consistent with a previous suture transplantation study[30].

Gli1+ cells are typical MSCs *in vitro*

The current definition of MSCs is based upon *in vitro* assays. Therefore, we evaluated *Gli1+* cells in accordance with these standards. Immunohistochemical staining indicated that the majority of *Gli1+* cells in the suture mesenchyme do not express MSC markers including CD90, CD73, CD44, Sca1, and CD146 (Figure 4a-f). CD44 expression was detectable in the osteogenic front region (Figure 4c), and Sca1 expression was detectable in the periosteum (Figure 4f). To study their *in vitro* properties, *Gli1-Cre^{ERT2};R26Tdtomato^{flox}* mice at 1 month of age were induced with tamoxifen. Mesenchymal cells were obtained from the suture one week after induction and cultured. FACS analysis indicated that *Gli1+* cells and their derivatives express high levels of typical MSC markers including CD44, CD90, Sca1, CD146, and CD73, but not CD34 (Figure 4g). Clonal culture indicated that *Gli1+* cells possess clone-forming ability (Figure 4h, k). Subculture of clones indicated that clones derived from single *Gli1+* cells are capable of osteogenic, chondrogenic and adipogenic differentiation (Figure 4i-l) and are therefore multipotent[31]. We compared the differentiation ability of suture MSCs with MSCs taken from femur bone marrow of the same mice. Although the osteogenic and chondrogenic differentiation abilities were comparable, the adipogenic differentiation ability of the suture MSCs was much weaker than that of the bone marrow MSCs (Figure 4m). These data indicate that although *Gli1+* cells do not express MSC markers *in vivo*, they behave like typical MSCs *in vitro* and are more committed towards osteochondrogenic lineages. Traditional MSC markers routinely used to identify MSCs *in vitro* are not ideal markers for MSCs *in vivo*.

Gli1+ stem cells are not associated with vasculature in the suture mesenchyme and are regulated by IHH from the osteogenic front

Previous studies have proposed that MSCs in the long bone are regulated by a perivascular niche[4]. We therefore set out to test whether *Gli1+* cells in the suture are regulated by the same mechanism. In fact, we found that *Gli1+* cells in the suture mesenchyme mainly reside around the midline of the structure and do not show a particular affinity for the vasculature (Figure 5a). After induction, *Shh-Cre^{ERT2};R26Tdtomato^{flox}* mice do not show any signal in the suture region (Figure 5b), indicating the absence of SHH from the suture mesenchyme, consistent with a previous study[32]. However, *Ihh-LacZ* reporter mice revealed *Ihh+* cells lining the edges of the calvarial bones (Figure 5c-d). *Ihh+* cells are positive for *Sp7* and *Runx2* (Figure 5e-f) and therefore can be deemed to reside within the osteogenic front in cranial sutures.

To investigate the function of *Hedgehog* signaling in regulating suture MSCs, we generated *Gli1-Cre^{ERT2};Smoothened$^{flox/flox}$* mice (*Smo ICKO*) and induced them at one month age. Blockage of the *Hh* pathway had no obvious impact on suture patency in these mice (Figure 5g-l). *Gli1+* cells could still give rise to periosteum, dura and osteocytes (Supplementary Figure 5p). However, all the craniofacial bones exhibited severe osteoporosis and reduced bone volume eight months after induction (Figure 5g-l). We also examined the continuously

growing incisors in *Smo ICKO* mice. We found that significant phenotypes appeared much sooner after induction in the incisors. Although the incisors continued growing, they showed significantly reduced odontogenesis and amelogenesis, disrupted odontoblast organization and severe periodontal ligament defects (Supplementary Figure 5a-l). Proliferation analysis indicated that loss of hedgehog signaling had no significant effects on the ratio of proliferating cells in either the incisor or sagittal suture (Supplementary Figure 5m-n). No apoptotic cells were detectable in the incisor or sagittal suture of control or Smo ICKO mice (Supplementary Figure 5o). To investigate the effects of hedgehog signaling, we harvested suture mesenchymal cells from one-month-old mice and treated them with IHH or hedgehog inhibitor GDC0449. IHH treatment (500ng/ml)[33] significantly up-regulated Gli1 activity, whereas GDC0449 (10μM)[34] significantly down-regulated Gli1 activity (Supplementary Figure 5q-s). Neither treatment had a significant effect on proliferation or apoptosis (Supplementary Figure 5t). Three weeks after treatment, osteogenic activity was increased in IHH-treated cells and decreased in GDC0449-treated cells (Supplementary Figure 5u-w). Real-time PCR also confirmed the opposing effects of IHH and GDC0449 on regulating the osteogenic differentiation ability of suture MSCs (Supplementary Figure 5x). These results indicate that *Hedgehog* signaling is important for regulating the differentiation of *Gli1+* MSCs but not for their maintenance.

Gli1+ cell ablation leads to craniosynostosis, skull growth arrest, osteoporosis and compromised injury repair

To investigate whether *Gli1+* stem cells are indispensable for homeostasis and injury repair, we generated *Gli1-Cre^{ERT2};DTA$^{flox/flox}$* mice (DTA) and induced them with tamoxifen at one month of age. Theoretically, induction should cause ablation of all *Gli1+* cells. We discovered that some *Gli1*-expressing cells survived the ablation, indicating that the DTA model we generated was not entirely efficient (Supplementary Figure 5z). However, even this incomplete *Gli1+* cell ablation led to striking craniofacial phenotypes. One month after induction, most sutures remain patent except the coronal and frontal-premaxilla sutures, suggesting these two sutures are more sensitive to *Gli1+* cell ablation (Figure 6b). Two months after induction, the general body size of the DTA mice was significantly smaller than that of controls of the same age and was comparable to one-month-old control mice, indicating the arrest of body growth after the ablation (Supplementary Figure 5y). In addition, all the craniofacial sutures had fused (Figure 6c-g). The anterior-posterior length and the width of the skull of the DTA mice were reduced by ~20% and 15%, respectively (Figure 6r). All the craniofacial bones exhibited severe osteoporosis (Figure 6h-m). Quantitative analysis of the volume of the maxillary bone, palatal bone and basosphenoid bone showed that all were reduced by over 40% (Figure 6r). HE staining confirmed the disappearance of the sagittal suture and coronal suture as well as the presence of porous bone structure (Figure 6n-q).

To evaluate the impact of *Gli1+* cell ablation on injury repair, we injured the calvarial bone of DTA mutants and controls one month after their induction. Although inspection of the control samples revealed that they had healed completely after one month, the injury sites in the DTA mutant calvarial bones remained open, indicating a compromised healing process (Figure 6s-t).

The stem cell population is diminished in the sutures of *Twist1*$^{+/-}$ mice with craniosynostosis

Our identification of *Gli1*+ stem cells in the craniofacial sutures and the craniosynostosis phenotype observed after *Gli1*+ cell ablation suggest that premature loss of stem cells from the suture causes the premature suture fusion observed in craniosynostosis.

To test this hypothesis, we generated *Twist1*$^{+/-}$;*Gli1-LacZ*$^{+/-}$ mice. *Twist1*$^{+/-}$ is a widely accepted synostosis mouse model and the corresponding mutation in humans is linked to Saethre-Chotzen syndrome, which is the most common craniosynostosis disorder[35-38]. Whole-mount LacZ staining of mice at one month of age indicated that the number of *Gli1*+ cells was significantly reduced (Figure 7 a-f). *Gli1*+ cells were not detectable in regions of fused coronal suture (Figure 7f-b'). Even in sutures of *Twist1*$^{+/-}$ mutants that remain patent, such as the coronal, lambdoid and sagittal sutures, the number of *Gli1*+ cells was reduced, and the reduction was more severe in the synostosed sutures (Figure 7d-g).

Next, we isolated suture mesenchymal cells from *Twist1*$^{+/-}$ mutants and littermate control calvarial bones. *In vitro* cultures indicated that both clone formation efficiency and clone size of *Twist1*$^{+/-}$ suture mesenchymal cells were reduced by over 50% (Figure 7h). Synostosis occurs between P9 and P13 in Twist1$^{+/-}$ mice[37, 39-41]. To investigate whether loss of Gli1+ cells occurs prior to suture closure, we examined Gli1 expression at P1, P7 and P14. Whole-mount LacZ staining indicated that Gli1+ cells in *Twist1*$^{+/-}$ mice at P1 did not differ significantly from controls in their number or distribution pattern (Figure 7i, l). At P7 and P14, Gli1+ cells were significantly reduced in all sutures of *Twist1*$^{+/-}$ mice (Figure 7j-k, m-n). To investigate the reduction in Gli1+ cells, we performed proliferation and apoptosis assays. EdU incorporation assays in P5 pups indicated that the number of proliferating cells in the sutures of *Twist1*$^{+/-}$ mice was reduced by nearly 50% (Figure 7o, q). At P5, discontinuous apoptotic cell foci were detectable in the coronal and lambdoid sutures of *Twist1*$^{+/-}$ mice, whereas no apoptotic cells were detectable in the sagittal sutures (Figure 8p)

Discussion

Our study shows that *Gli1*+ cells in the suture mesenchyme are stem cells for craniofacial bones. They give rise to the osteogenic front, periosteum, dura and craniofacial bones (Supplementary figure 6a). The *Gli1*+ population provides an indispensable stem cell source supporting craniofacial bone turnover and injury repair in the adult. These *Gli1*+ cells can be considered osteogenic stem cells because they largely or perhaps exclusively give rise to bone tissue; craniofacial bones contain few chondrocytes except in the basal skull and nasal septum. The periosteum and dura are mainly comprised of committed osteogenic progenitors, as evidenced by their high expression of differentiation markers, and these tissues derive from the suture (Supplementary figure 6a).

Gli1 is specifically expressed within the suture mesenchyme but not in hematopoietic cells or endothelium[26]. *Gli1*+ cells in the suture mesenchyme are not perivascular, as tendon stem cells are[42, 43]. IHH secreted from progeny cells in the osteogenic front regulates the differentiation of *Gli1*+ MSCs within the suture (Supplementary figure 6 b). Hedgehog

signaling is not critical for stem cell maintenance, as previously shown in incisors and long bones[26, 44, 45]. Craniofacial bones contain limited bone marrow space and the *Gli1*+ cells within the marrow also contribute to new bone formation. Their contribution to craniofacial bones is less significant than that of the suture MSCs based on our transplantation experiments and their small population size.

Ablation of *Gli1*+ cells leads to fusion of all craniofacial sutures in adult mice. The fusion might be due to the loss of a constant stem cell supply that is needed to produce sufficient undifferentiated mesenchymal cells to keep the suture patent. Combining the craniosynostosis phenotypes after *Gli1*+ cell ablation with the reduced *Gli1*+ cell numbers observed in *Twist1*$^{+/-}$ sutures, we propose a mechanism for explaining craniosynostosis, namely that premature loss of MSCs from a craniofacial suture can contribute to craniosynostosis. This concept of the disease will have a profound impact on our approach to diagnosis, prevention and treatment of craniosynostosis. *Twist1* is specifically expressed in the suture mesenchyme after E16[41]. *Twist1*$^{+/-}$ mice exhibit increased apoptosis and reduced proliferation within the suture mesenchyme[46, 47], likely resulting in the reduced *Gli1*+ cells that we reported. It appears that there is a threshold number of suture stem cells required for maintaining suture patency. This may help to explain the often-asymmetrical nature of craniosynostosis.

In summary, we have identified *Gli1*+ cells within the suture mesenchyme as an indispensable MSC population supporting craniofacial bone turnover and injury healing. These stem cells are not associated with vasculature and are regulated by IHH secreted from the osteogenic front. *Gli1*+ cells in the suture mesenchyme do not express conventional MSC markers *in vivo;* their derivatives *in vitro*, however, express all these markers and behave like typical MSCs[26, 48-50]. Collectively, our study will have a profound impact on the understanding of craniofacial bones as well as the pathogenesis of craniosynostosis and other craniofacial disorders.

Methods

Histology

Samples were dissected under a stereomicroscope (Leica L2) and fixed in 4% paraformaldehyde overnight at room temperature, then decalcified in 20% EDTA for 14 days. Decalcified samples were dehydrated in 60% sucrose/PBS solution overnight at room temperature. Samples were embedded in an OCT compound (TissuTek, Sakura) under a stereomicroscope and transferred onto dry ice to solidify. Embedded samples were cryosectioned at 16 μm thickness using a cryostat (Leica CM1850). Images were captured using a fluorescence microscope (Leica DMI 3000B) with filter settings for DAPI/FITC/TRITC and merged with Adobe Photoshop CS6. Confocal images were acquired using Leica LAS AF software (Leica) with lasers and corresponding band-pass filters for DAPI (Ex. 405 nm, BP410-490), GFP (Ex. 488 nm, BP450-550), tdTomato (Ex. 543 nm, BP550-595) and Alexa633 (Ex. 633 nm, LP650). Adobe Photoshop software was used to capture and align images. Representative images from at least three independent samples or experiments are shown in the figures (see Reproducibility of experiments).

Tamoxifen administration

Tamoxifen (Sigma T5648) was suspended in corn oil (Sigma C8267) at 20 mg/ml and injected intraperitoneally (i.p.) at a dosage of 10 mg daily for 4 days.

EdU incorporation and TUNEL assays

EdU (200 mg/kg) (Life Technology A10044) was injected i.p. 2 hours prior to sacrifice. The specimens were fixed overnight in 4% PFA and decalcified in 20% EDTA for 2 weeks. Tissues were embedded in OCT compound (Sakura Tissue-Teck 4583), frozen, and sectioned at 12–18 μm thickness. EdU+ cells were detected with the Click-iT® EdU Alexa Fluor® 488 Imaging Kit (Invitrogen C10337) according to the recommended protocol. Apoptotic cells were detected with the In Situ Cell Death Detection Kit (Roche Life Science 11684795910) according to the recommended protocol. For quantification of EdU+ or TUNEL+ cells, we counted the number of nuclei marked by staining in each section.

Suture transplantation

Our surgical protocol was adapted from a previous study[51]. After sacrificing donor mice, a section of sagittal suture 2mm in length was dissected together with ~0.5mm of abutting parietal bone on each side. The periosteum and dura were either preserved or carefully removed with a scalpel depending on the experimental design. Each transplant was imaged under a microscope before transplantation to measure its initial size. Nude mice were used as the recipient mice. Under general anesthesia, a midline sagittal skin incision was made and a scalp flap was elevated to reveal the calvaria. The periosteum was retracted over the left and right parietal bones from the mid-sagittal incision to expose the underlying bone. A $4mm^2$ defect was made in the center of the left or right parietal bone of the host using a hand-held drill (NSK Z500). Extreme care was taken not to damage the underlying dura. Donor transplants were placed over the recipient calvarial window with the dura side facing the brain. No additional fixation was necessary. The host skin was sutured using 4.0 nylon stitches.

Suture and calvarial bone injury assays

In the suture injury assay, a midline sagittal incision was made under general anesthesia and the scalp was revealed to expose the sagittal suture. A 25 gauge needle was used to scratch the sagittal suture surface. The scalp was then sutured together with 4.0 nylon stitches. In the calvarial bone injury assay, the scalp was cut and elevated to expose the parietal bones. A dental round burr was used to drill a hole of ~1mm diameter 2mm away from the sagittal suture in the parietal bone. The scalp was then sutured with silk stitches.

Statistical analysis

SPSS software version 13.0 was used for statistical analysis. Significance was assessed using independent two-tailed Student's *t*-tests or analysis of variance (ANOVA). A p value less than 0.05 was considered significant. No statistical method was used to predetermine sample size. The experiments were not randomized. The investigators were not blinded to allocation during experiments and outcome assessment.

Immunohistochemical staining

The following antibodies were used in our study: β-Gal (Novus NP600-305, 1:50), Gli1 (Novus Biological NBP1-78259, 1:25), CD44 (BD Bioscience 561859, clone IM7, 1:100), CD73 (BD Bioscience 561545 clone TY/23, 1:100), CD 105 (BD Bioscience 561443, clone266, 1:100), CD146 (BD Bioscience 562229, cloneME-9F1, 1:100), Sca1 (BD Bioscience 561077, clone E13-161.7, 1:100), Sp7 (Abcam ab22552, 1:100), Runx2 (Abcam ab61753, 1:100), Osteocalcin (Abcam ab93876), perilipin (Abcam ab3526, 1:100). Staining was performed according to standard procedures. The data from immunohistochemical staining experiments were representatives of 3 independent experiments (see Reproducibility of experiments).

Real-time PCR

The mRNA levels of *ALPase, Runx2, Sp7* and *Osteocalcin* were analyzed by real-time quantitative RT-PCR. Cells were collected from the culture dishes and total RNA was extracted using the RNeasy Mini Kit (Qiagen 74104). 1 μg total RNA was reverse-transcribed with oligo-dT primers into cDNAs using SuperScript™ III First-Strand (Invitrogen #18080-051). Real-time PCR was performed using a SYBR super mix kit (Bio-Rad #170-8880) as reported previously[52]. For thermal cycling, a CFX96 Real-Time System (Bio-Rad iCycler) was used at 95°C for 10min then 40 cycles of 95°C for 10 seconds and 55°C for 30 seconds. The relative amount of each mRNA transcript was calculated based on a standard curve of cycle thresholds and normalized to *β-actin* expression as the internal control. Real-time PCR was performed in triplicate for each sample. All experiments were repeated three times. The primers are as follows: mouse *β-actin*, 5′-GCAAGTGCTTCTAGGCGGAC-3′ and 5′- AAGAAAGGGTGTAAAACGCAGC-3′; mouse *ALPase*, 5'-GCTGATCATTCCCACGTTTT-3' and 5'-CTGGGCCTGGTAGTTGTTGT-3'; mouse *Runx2*, 5'-CCCAGCCACCTTTACCTACA- 3' and 5'-TATGGAGTGCTGCTGGTCTG-3'; mouse *Sp7*, 5'-AGTTCACCTGCCTGCTCTGT-3' and 5'-GGAGCTGGAGACCTTCCTCT-3'; mouse *Osteocalcin*, 5'-AAGCAGGAGGGCAATAAGGT-3' and 5'-ACTTGCAGGGCAGAGAGAGA-3'.

X-gal staining

Samples from mice were fixed in 0.2% glutaraldehyde overnight and then decalcified with 20% EDTA for 2 weeks. Frozen sections were cut of 12 μm thickness. Sections or cultured cells were stained with X-gal ($C_{14}H_{15}BrClNO_6$, USB) overnight at 37°C according to standard procedure.

Suture mesenchymal cell mass culture, clonal culture and multipotential differentiation

Our suture mesenchymal cell culture procedure was adopted from previous studies[31, 53]. After removing the periosteum and dura, the sagittal suture was excised along with ~0.5mm of abutting parietal bone on each side. The suture tissue was minced into tiny pieces and the tissue blocks were transferred into a T25 culture flask (Corning **CLS430639**) and incubated with αMEM+20% FBS (Invitrogen 10437-085) at 37°C in regular atmospheric conditions. For clonal culture of suture mesenchymal cells, 1000 cells from the sagittal suture

mesenchyme were plated in a T75 culture flask (Corning CLS430641) coated with fibronectin (Invitrogen 33010- 018) and incubated with αMEM+20% FBS (Invitrogen 10437-085) at 37°C under hypoxic conditions (5% O_2, 5% CO_2, balanced with Nitrogen). Clones could be detected ~10 days after plating. Single clones were circled with a cloning ring and digested with TrypLE (Invitrogen 12605). Cells were divided and plated into three wells in a fibronectin-coated 24-well culture plate (Corning CLS3527) and cultured under hypoxic conditions until confluence. Osteogenic, adipogenic or chondrogenic differentiation was then performed as previously described[54].

Flow cytometry analysis

Cultured suture mesenchymal cells of p0 or p1 were dissociated into single cells by treating the cells with 0.25% trypsin (Life Technology, 25200-056) for 40 min at 37°C and vigorous pipetting. Cells were then filtered with a 35 μm cell strainer (BD Falcon, 352235) to remove the residual cell mass. Cell suspensions were stained with FITC-conjugated antibodies for 30 min at 4°C followed by extensive washing with PBS. The following antibodies were used at 1:30 dilution: CD34 (BD Bioscience 560238, clone RAM34), CD44 (BD Bioscience 561859, clone IM7), CD45 (BD Bioscience 553080, clone 30-F11), CD73 (BD Bioscience 561545 clone TY/23), CD105 (BD Bioscience 561443, clone266), CD146 (BD Bioscience 562229, cloneME-9F1), Sca1 (BD Bioscience 561077, clone E13-161.7), IgG1 (BD Bioscience 554679, clone MOPC-21), IgG2a (BD Bioscience 553929, clone R35-95) and IgG2b (BD Bioscience 557726, clone A95-1) isotype control of IgG. Flow cytometry analysis was performed according to standard procedures as previously described[54]. All samples were analyzed with FACS^{calibur} (BD Bioscience).

Animal information

We obtained the following mouse strains from the Jackson Laboratory: *Shh-Cre^{ERT2}* (JAX# 005623)[55], *Gli1-LacZ* (JAX#008211)[56], Nude (JAX#007850), *Gli1-Cre^{ERT2}* (JAX#007913)[57], *ROSA26$^{LoxP\text{-}STOP\text{-}LoxP\text{-}ZsGreen1}$*(JAX#007906)[58], *ROSA26$^{LoxP\text{-}STOP\text{-}LoxP\text{-}DTA}$* (JAX#009669)[59], *Smo$^{flox/flox}$* (JAX#004526)[60], *ROSA26$^{LoxP\text{-}STOP\text{-}LoxP\text{-}Tdtomato}$* (JAX#007905)[58], *ROSA26$^{LoxP\text{-}STOP\text{-}LoxPLacZ}$* (JAX#003474)[61] and *CAG-EGFP* (JAX#003516)[62]. *Ihh-LacZ* mice were kindly provided by Andrew McMahon. Mouse experiments were approved by the University of Southern California Institutional Animal Care and Use Committee and performed following the regulations for animal experiments at University of Southern California. All mice were housed in a pathogen-free condition and analyzed in a mixed background. Mice were identified by ear tags. Tail biopsies of mice were lysed by incubating the tail sample at 55°C overnight in DirectPCR tail solution (Viagen 102-T) followed by 85°C heat inactivation for 30 minutes and used for PCR-based genotyping (GoTaq Green Master Mix, Promega, and C1000 Touch Cycler, Bio-rad). Mice were euthanized by carbon dioxide or decapitation. All mice were used for analysis regardless of sex.

For the experiments in Figure 1a–p, male *Gli1-LacZ* mice were mated to female CD1 mice (>8 weeks old, Jackson Lab) and vaginal plugs were checked the next morning. Newborn pups were counted as P0. Mice at indicated ages were collected and genotyped.

For experiments in Figure 2a-i, *Gli1-Cre^{ERT2};ROSA26$^{LoxP-STOP-LoxP-ZsGreen1}$* mice of mixed background were injected with tamoxifen at one month of age. Samples were collected at indicated time points after induction.

For the experiments in Figure 3a-d, *Gli1-LacZ* or *Gli1-Cre^{ERT2};ROSA26$^{LoxP-STOP-LoxP-ZsGreen1}$* mice of mixed background were injured at one month age. For experiments in Figure 3e-i, calvaria or suture transplants were obtained from one-month-old donor mice and transplanted into one-month-old nude mice.

For experiments in Figure 4a-f, one-month-old *Gli1-LacZ* mice were used for analysis. For experiments in figure 4g-l, one-month-old *Gli1-Cre^{ERT2};ROSA26$^{LoxP-STOP-LoxP-Tdtomato}$* mice were used for cell culture.

For experiments in Figure 5a-f, one-month-old mice were used for analysis. For experiments in Figure 5g-l, one-month-old *Gli1-Cre^{ERT2};Smo$^{flox/flox}$* mice were induced with tamoxifen and samples were collected at indicated time points after induction.

For experiments in Figure 6a-t, *Gli1-CreERT2;ROSA26LoxP$^{-STOP-LoxP-DTA}$* or *DTA $^{flox/flox}$* mice were induced with tamoxifen at one month of age. Samples were collected at indicated time points after induction.

For experiments in Figure 7a-p, male *Twist1*+/− mice were mated with female *Gli1-LacZ*+/− mice to generate *Twist1*+/−;*Gli1-LacZ*+/− mice. Samples were collected at indicated ages.

For experiments in Supplementary Figures 1d-f and 2a-o, 2q, mice of indicated genotypes were collected at one month of age. For experiments in Supplementary Figure 2p, *Gli1-LacZ* +/− pups of P8 were collected for experiments.

For experiments in Supplementary Figure 3a-o', one-month-old *Gli1-Cre^{ERT2};ROSA26$^{LoxP-STOP-LoxP-Tdtomato}$* mice were induced with tamoxifen and samples were collected at indicated time points after induction.

For experiments in Supplementary Figure 4 a-b, one-month-old *Gli1-LacZ* mice were used for analysis. For experiments in Supplementary Figure 4c-d, one-month-old *Gli1-Cre^{ERT2};ROSA26$^{LoxP-STOP-LoxP-Tdtomato}$* mice were induced and samples were collected at indicated time points.

For experiments in Supplementary Figure 5a-p, one-month-old *Gli1-Cre^{ERT2};Smo$^{flox/flox}$* mice were induced with tamoxifen and samples were collected at indicated time points after induction. For experiments in Supplementary Figure 5q-x, one-month-old *Gli1-LacZ* mice were used for harvesting suture MSCs. For experiments in Supplementary Figure 5y-z, one-month-old *Gli1-CreERT2;ROSA26LoxP$^{-STOP-LoxP-DTA}$* mice were induced with tamoxifen.

Reproducibility of experiments

Figure 3i shows representative data from 12 independent experiments. Figures 6a-q and 7a-f show representative data from 10 independent experiments. Figure 7o-p show representative

data from 6 independent experiments. Figures 1a-p, 2a-i,3e-h, 4h-m, 5g-l, 7i-n and Supplementary Figures 2a-m, 3a-n, 3a'-o', 4a-d and 5a-p show representative data from 5 independent experiments. Supplementary Figure 5q-z show representative data from 4 independent experiments. Figures 1q-t, 3a-d, 4a-g, 5a-f, 6s-t and Supplementary Figures 1a-f and 2n-q show representative data from 3 independent experiments.

Supplementary Material

Refer to Web version on PubMed Central for supplementary material.

Acknowledgements

We thank Julie Mayo, Bridget Samuels for critical reading of the manuscript and Meng Zhang for the support. We thank Ruili Yang, Xingtian Xu and Songtao Shi for technical support on the FACS analysis. We thank Andrew McMahon for providing *Ihh-LacZ* mice. Hu Zhao acknowledges training grant support from the National Institute of Dental and Craniofacial Research, NIH (R90 DE022528). This study was supported by grants from the National Institute of Dental and Craniofacial Research, NIH (DE022503, DE020065 and DE012711) to Yang Chai.

References

1. Chai Y, Maxson RE Jr. Recent advances in craniofacial morphogenesis. Dev Dyn. 2006; 235:2353–2375. [PubMed: 16680722]
2. Clark BR, Keating A. Biology of bone marrow stroma. Annals of the New York Academy of Sciences. 1995; 770:70–78. [PubMed: 8597383]
3. Riminucci M, Remoli C, Robey PG, Bianco P. Stem cells and bone diseases: New tools, new perspective. Bone. 2015; 70C:55–61. [PubMed: 25240458]
4. Zhou BO, Yue R, Murphy MM, Peyer JG, Morrison SJ. Leptin-receptor-expressing mesenchymal stromal cells represent the main source of bone formed by adult bone marrow. Cell Stem Cell. 2014; 15:154–168. [PubMed: 24953181]
5. Mendez-Ferrer S, et al. Mesenchymal and haematopoietic stem cells form a unique bone marrow niche. Nature. 2010; 466:829–834. [PubMed: 20703299]
6. Worthley DL, et al. Gremlin 1 identifies a skeletal stem cell with bone, cartilage, and reticular stromal potential. Cell. 2015; 160:269–284. [PubMed: 25594183]
7. Grayson WL, et al. Stromal cells and stem cells in clinical bone regeneration. Nat Rev Endocrinol. 2015
8. Yang M, Zhang H, Gangolli R. Advances of mesenchymal stem cells derived from bone marrow and dental tissue in craniofacial tissue engineering. Current stem cell research & therapy. 2014; 9:150–161. [PubMed: 24524798]
9. Robey PG. Cell sources for bone regeneration: the good, the bad, and the ugly (but promising). Tissue engineering. Part B, Reviews. 2011; 17:423–430. [PubMed: 21797663]
10. Lin Z, Fateh A, Salem DM, Intini G. Periosteum: biology and applications in craniofacial bone regeneration. J Dent Res. 2014; 93:109–116. [PubMed: 24088412]
11. Ochareon P, Herring SW. Cell replication in craniofacial periosteum: appositional vs. resorptive sites. J Anat. 2011; 218:285–297. [PubMed: 21223257]
12. Pagni G, et al. Bone repair cells for craniofacial regeneration. Advanced drug delivery reviews. 2012; 64:1310–1319. [PubMed: 22433781]
13. Petrovic V, Zivkovic P, Petrovic D, Stefanovic V. Craniofacial bone tissue engineering. Oral surgery, oral medicine, oral pathology and oral radiology. 2012; 114:e1–9.
14. Badve CA, K MM, Iyer RS, Ishak GE, Khanna PC. Craniosynostosis: imaging review and primer on computed tomography. Pediatric radiology. 2013; 43:728–742. quiz 725-727. [PubMed: 23636536]
15. Senarath-Yapa K, et al. Craniosynostosis: molecular pathways and future pharmacologic therapy. Organogenesis. 2012; 8:103–113. [PubMed: 23249483]

16. Levi B, et al. Cranial suture biology: from pathways to patient care. J Craniofac Surg. 2012; 23:13–19. [PubMed: 22337368]
17. Slater BJ, et al. Cranial sutures: a brief review. Plast Reconstr Surg. 2008; 121:170e–178e.
18. Lattanzi W, et al. Genetic basis of single-suture synostoses: genes, chromosomes and clinical implications. Childs Nerv Syst. 2012; 28:1301–1310. [PubMed: 22872241]
19. Ciurea AV, Toader C. Genetics of craniosynostosis: review of the literature. Journal of medicine and life. 2009; 2:5–17. [PubMed: 20108486]
20. Martou G, Antonyshyn OM. Advances in surgical approaches to the upper facial skeleton. Current opinion in otolaryngology & head and neck surgery. 2011; 19:242–247. [PubMed: 21659880]
21. Posnick JC, Tiwana PS, Ruiz RL. Craniofacial dysostosis syndromes: evaluation and staged reconstructive approach. Atlas of the oral and maxillofacial surgery clinics of North America. 2010; 18:109–128. [PubMed: 21036313]
22. Hankinson TC, Fontana EJ, Anderson RC, Feldstein NA. Surgical treatment of single-suture craniosynostosis: an argument for quantitative methods to evaluate cosmetic outcomes. Journal of neurosurgery. Pediatrics. 2010; 6:193–197. [PubMed: 20672943]
23. Forrest CR, Hopper RA. Craniofacial syndromes and surgery. Plast Reconstr Surg. 2013; 131:86e–109e.
24. Tatum SA, Losquadro WD. Advances in craniofacial surgery. Archives of facial plastic surgery. 2008; 10:376–380. [PubMed: 19018057]
25. Wan DC, Kwan MD, Lorenz HP, Longaker MT. Current treatment of craniosynostosis and future therapeutic directions. Frontiers of oral biology. 2008; 12:209–230. [PubMed: 18391503]
26. Zhao H, et al. Secretion of shh by a neurovascular bundle niche supports mesenchymal stem cell homeostasis in the adult mouse incisor. Cell Stem Cell. 2014; 14:160–173. [PubMed: 24506883]
27. Behr B, Longaker MT, Quarto N. Absence of endochondral ossification and craniosynostosis in posterior frontal cranial sutures of Axin2(−/−) mice. PLoS One. 2013; 8:e70240. [PubMed: 23936395]
28. Bajwa M, et al. Normal fusion of the metopic suture. J Craniofac Surg. 2013; 24:1201–1205. [PubMed: 23851769]
29. Stotland MA, Do NK, Knapik TJ. Bregmatic wormian bone and metopic synostosis. J Craniofac Surg. 2012; 23:2015–2018. [PubMed: 23154373]
30. Slater BJ, Lenton KA, James A, Longaker MT. Ex vivo model of cranial suture morphogenesis and fate. Cells Tissues Organs. 2009; 190:336–346. [PubMed: 19590164]
31. Xu Y, Malladi P, Chiou M, Longaker MT. Isolation and characterization of posterofrontal/sagittal suture mesenchymal cells in vitro. Plast Reconstr Surg. 2007; 119:819–829. [PubMed: 17312483]
32. Lenton K, et al. Indian hedgehog positively regulates calvarial ossification and modulates bone morphogenetic protein signaling. Genesis. 2011; 49:784–796. [PubMed: 21557453]
33. Kim EJ, et al. Ihh and Runx2/Runx3 signaling interact to coordinate early chondrogenesis: a mouse model. PLoS One. 2013; 8:e55296. [PubMed: 23383321]
34. Singh BN, Fu J, Srivastava RK, Shankar S. Hedgehog signaling antagonist GDC-0449 (Vismodegib) inhibits pancreatic cancer stem cell characteristics: molecular mechanisms. PLoS One. 2011; 6:e27306. [PubMed: 22087285]
35. Grova M, et al. Models of cranial suture biology. J Craniofac Surg. 2012; 23:1954–1958. [PubMed: 23154351]
36. Howard TD, et al. Mutations in TWIST, a basic helix-loop-helix transcription factor, in Saethre-Chotzen syndrome. Nat Genet. 1997; 15:36–41. [PubMed: 8988166]
37. Behr B, Longaker MT, Quarto N. Craniosynostosis of coronal suture in twist1 mice occurs through endochondral ossification recapitulating the physiological closure of posterior frontal suture. Frontiers in physiology. 2011; 2:37. [PubMed: 21811467]
38. Jezela-Stanek A, Krajewska-Walasek M. Genetic causes of syndromic craniosynostoses. European journal of paediatric neurology : EJPN : official journal of the European Paediatric Neurology Society. 2013; 17:221–224. [PubMed: 23062756]
39. Paznekas WA, et al. Genetic heterogeneity of Saethre-Chotzen syndrome, due to TWIST and FGFR mutations. American journal of human genetics. 1998; 62:1370–1380. [PubMed: 9585583]

40. el Ghouzzi V, et al. Mutations of the TWIST gene in the Saethre-Chotzen syndrome. Nat Genet. 1997; 15:42–46. [PubMed: 8988167]
41. Rice DP, et al. Integration of FGF and TWIST in calvarial bone and suture development. Development. 2000; 127:1845–1855. [PubMed: 10751173]
42. Bi Y, et al. Identification of tendon stem/progenitor cells and the role of the extracellular matrix in their niche. Nat Med. 2007; 13:1219–1227. [PubMed: 17828274]
43. Hogan MV, et al. Tissue engineering solutions for tendon repair. The Journal of the American Academy of Orthopaedic Surgeons. 2011; 19:134–142. [PubMed: 21368094]
44. Seidel K, et al. Hedgehog signaling regulates the generation of ameloblast progenitors in the continuously growing mouse incisor. Development. 2010; 137:3753–3761. [PubMed: 20978073]
45. Pan A, Chang L, Nguyen A, James AW. A review of hedgehog signaling in cranial bone development. Frontiers in physiology. 2013; 4:61. [PubMed: 23565096]
46. Yousfi M, Lasmoles F, El Ghouzzi V, Marie PJ. Twist haploinsufficiency in Saethre-Chotzen syndrome induces calvarial osteoblast apoptosis due to increased TNFalpha expression and caspase-2 activation. Human molecular genetics. 2002; 11:359–369. [PubMed: 11854168]
47. Miraoui H, Marie PJ. Pivotal role of Twist in skeletal biology and pathology. Gene. 2010; 468:1–7. [PubMed: 20696219]
48. Bianco P. Stem cells and bone: A historical perspective. Bone. 2015; 70C:2–9. [PubMed: 25171959]
49. Keating A. Mesenchymal stromal cells: new directions. Cell Stem Cell. 2012; 10:709–716. [PubMed: 22704511]
50. Tolar J, Le Blanc K, Keating A, Blazar BR. Concise review: hitting the right spot with mesenchymal stromal cells. Stem Cells. 28:1446–1455. [PubMed: 20597105]
51. Opperman LA, Sweeney TM, Redmon J, Persing JA, Ogle RC. Tissue interactions with underlying dura mater inhibit osseous obliteration of developing cranial sutures. Dev Dyn. 1993; 198:312–322. [PubMed: 8130378]
52. Oka K, et al. The role of TGF-beta signaling in regulating chondrogenesis and osteogenesis during mandibular development. Dev Biol. 2007; 303:391–404. [PubMed: 17204263]
53. James AW, Xu Y, Wang R, Longaker MT. Proliferation, osteogenic differentiation, and fgf-2 modulation of posterofrontal/sagittal suture-derived mesenchymal cells in vitro. Plast Reconstr Surg. 2008; 122:53–63. [PubMed: 18594386]
54. Chung IH, et al. Stem cell property of postmigratory cranial neural crest cells and their utility in alveolar bone regeneration and tooth development. Stem Cells. 2009; 27:866–877. [PubMed: 19350689]
55. Harfe BD, et al. Evidence for an expansion-based temporal Shh gradient in specifying vertebrate digit identities. Cell. 2004; 118:517–528. [PubMed: 15315763]
56. Bai CB, Auerbach W, Lee JS, Stephen D, Joyner AL. Gli2, but not Gli1, is required for initial Shh signaling and ectopic activation of the Shh pathway. Development. 2002; 129:4753–4761. [PubMed: 12361967]
57. Ahn S, Joyner AL. Dynamic changes in the response of cells to positive hedgehog signaling during mouse limb patterning. Cell. 2004; 118:505–516. [PubMed: 15315762]
58. Madisen L, et al. A robust and high-throughput Cre reporting and characterization system for the whole mouse brain. Nat Neurosci. 2010; 13:133–140. [PubMed: 20023653]
59. Voehringer D, Liang HE, Locksley RM. Homeostasis and effector function of lymphopenia-induced “memory-like” T cells in constitutively T cell-depleted mice. J Immunol. 2008; 180:4742–4753. [PubMed: 18354198]
60. Long F, Zhang XM, Karp S, Yang Y, McMahon AP. Genetic manipulation of hedgehog signaling in the endochondral skeleton reveals a direct role in the regulation of chondrocyte proliferation. Development. 2001; 128:5099–5108. [PubMed: 11748145]
61. Soriano P. Generalized lacZ expression with the ROSA26 Cre reporter strain. Nat Genet. 1999; 21:70–71. [PubMed: 9916792]

62. Hadjantonakis AK, Gertsenstein M, Ikawa M, Okabe M, Nagy A. Generating green fluorescent mice by germline transmission of green fluorescent ES cells. Mechanisms of development. 1998; 76:79–90. [PubMed: 9867352]

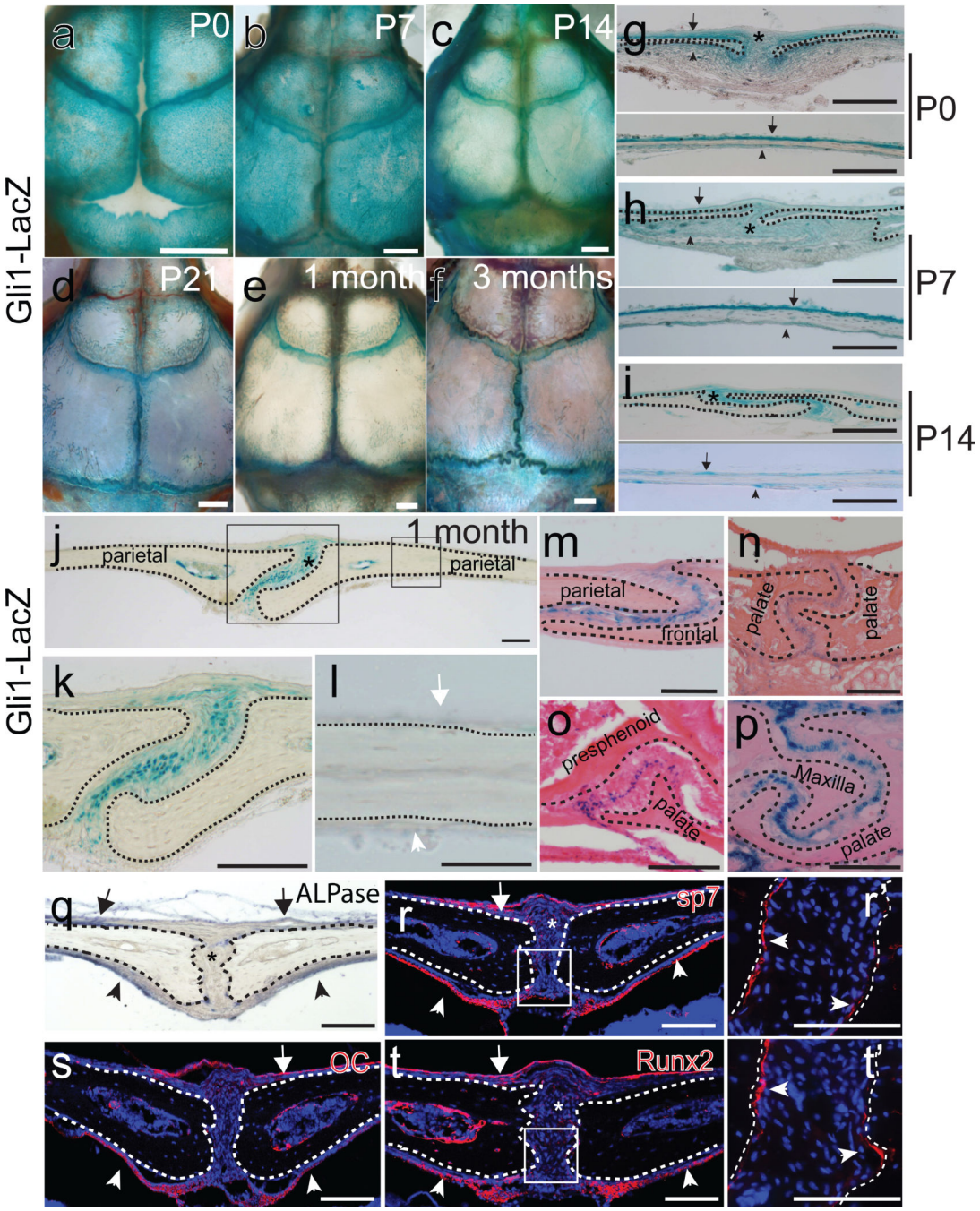

Figure 1.

Gli1+ cells are restricted to the suture mesenchyme of craniofacial bones and are undifferentiated cells. (a-f) Whole mount LacZ staining (blue) of calvarial bones of newborn (P0), 7, 14 and 21 day old (P7, P14, P21) and one- and three-month-old *Gli1-LacZ* mice. (g-i) LacZ staining of sections of sagittal sutures and parietal bones of P0, P7 and P14 mice indicates *Gli1+* cells are present in the suture mesenchyme (asterisks), periosteum (arrows) and dura (arrowheads). (j-l) LacZ staining of sections of the sagittal suture of one-month-old *Gli1-LacZ* mice. Asterisk indicates exclusive Gli1 expression within the suture

mesenchyme. No positive staining is detectable in the periosteum (white arrow) and dura (white arrowhead). Boxed areas in j are displayed in k and l. (m-p) LacZ staining of the mid-suture mesenchyme in the coronal (m), interpalatal (n), presphenoid-palatal (o) and maxilla-palatal (p) sutures of one-month-old *Gli1-LacZ* mice. (q-t) ALPase (blue) and immunohistochemical (red) staining of sagittal sutures of one-month-old mice. Osteogenic markers including *ALPase* (q), *Sp7* (r), *osteocalcin(OC)* (s) and *Runx2* (t) are not detectable in the suture mesenchyme (asterisks). The periosteum (arrows) and dura (arrowheads) strongly express these markers. Boxed areas in r and t are enlarged in panels r' and t', respectively, showing positive expression in the osteogenic fronts (arrowheads). Dotted lines outline margins of craniofacial bones. Scale bars in panels a-f, 1mm; other scale bars, 100 μm.

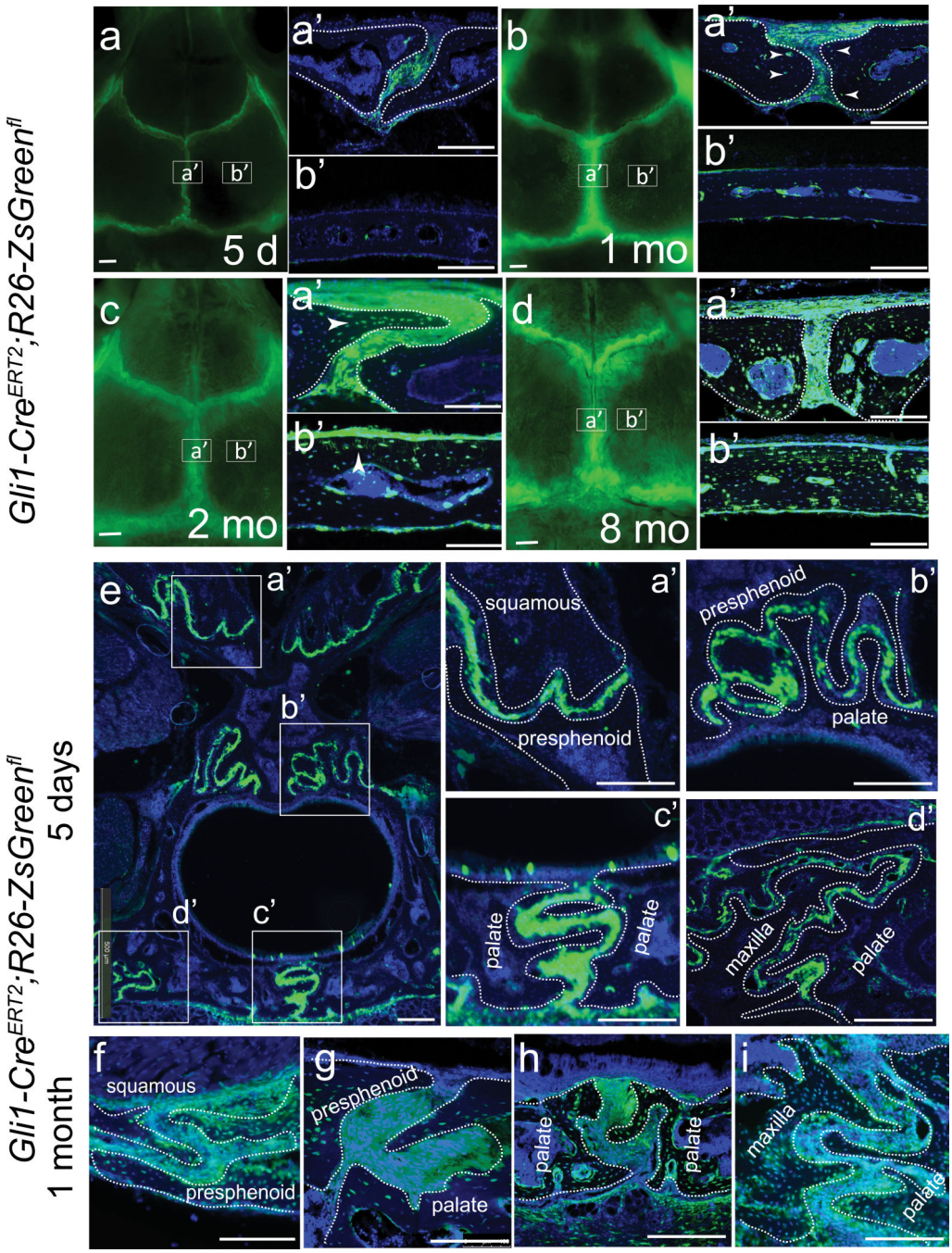

Figure 2.

Gli1+ cells in the suture mesenchyme contribute to adult craniofacial bone turnover. *Gli1-CE;R26ZsGreen*^{fl} mice were induced at 1 month of age with tamoxifen. (a-d) Gli1+ cells in the adult sagittal suture mesenchyme 5 days and 1, 2 and 8 months after induction. Arrowheads indicate positively labeled osteocytes. Boxes indicate the approximate positions of sections shown in the right panels (a' and b'). (e-i) Five days (e, a'-d') and one month (f-i) after induction, fluorescently labeled cells are detectable in the craniofacial sutures (low magnification image in e) including the squamous-presphenoid (panels a', f), presphenoid-

palatal (panels b', g), interpalatal (panels c', h) and maxilla-palatal (panels d', i) sutures. Dotted lines outline craniofacial bones. Scale bars in panel a-d, 1mm; other scale bars, 100 μm.

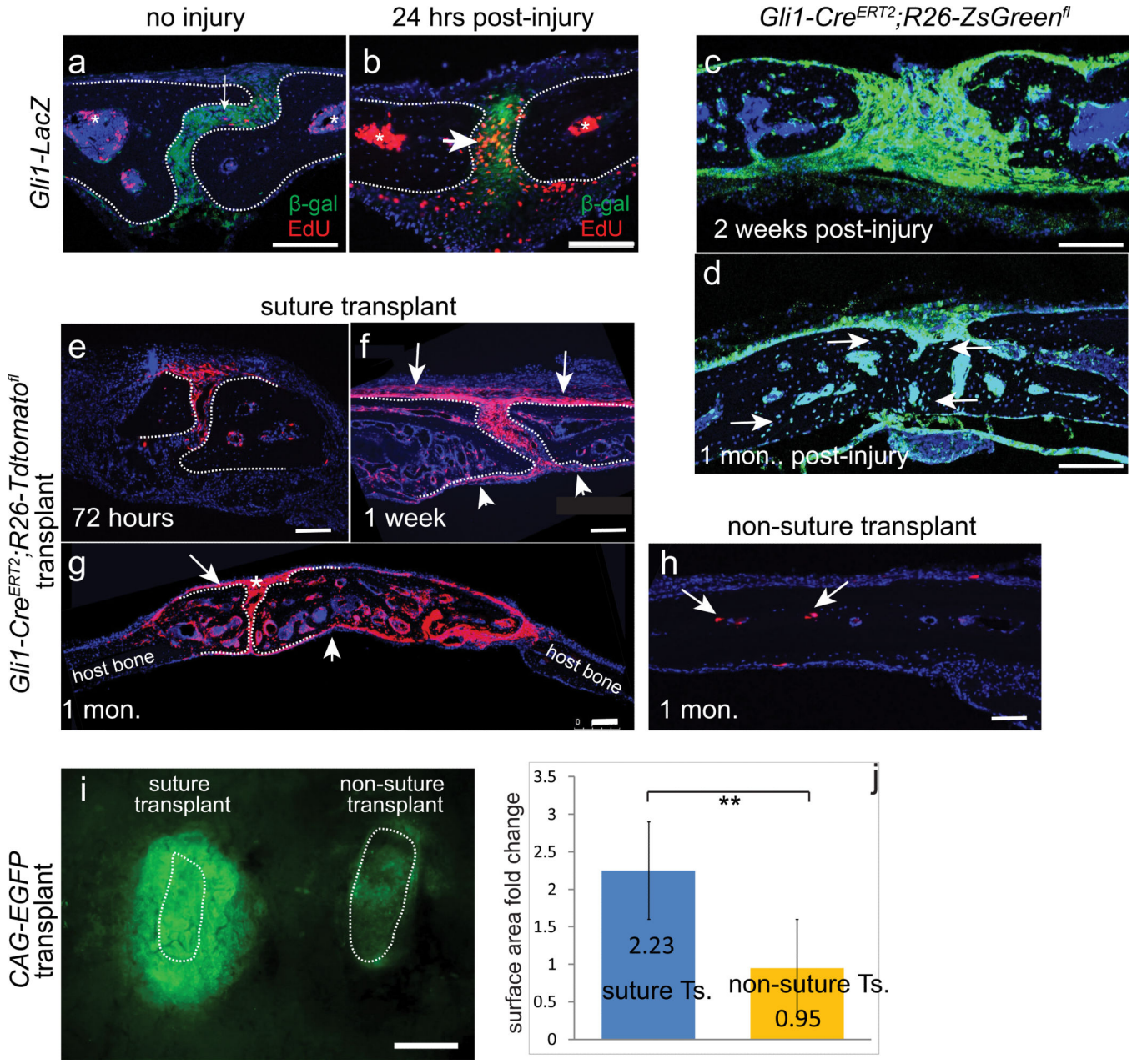

Figure 3.

Gli1+ cells in the suture mesenchyme contribute to injury repair and support transplant growth. (a,b) EdU incorporation (red) in the suture mesenchyme of Gli1-LacZ (green) mice uninjured or twenty-four hours after injury. Post-injury, many Gli1+ cells are activated into proliferation (arrow in b). Asterisks indicate proliferating blood cells in the bone marrow space. Dotted lines outline margins of parietal bones. (c,d) Visualization of sutures in *Gli1-CE;R26*^{ZsGreen} mice two weeks and one month after induction with tamoxifen at 1 month of age and injury five days later. Arrows indicate fluorescently labeled osteocytes in the reparative region. (e-g) Transplantation of sagittal sutures without the periosteum and dura from *Gli1-CE;R26-Tdtomato*^{fl} mice into nude mice. Samples collected 72 hours (e), 1 week

(f) and 1 month (g) after transplantation indicate *Gli1+* cells in the suture mesenchyme gradually contribute to the formation of new periosteum (arrows), new dura (arrowheads) and new bone. Asterisk indicates patent suture in the transplant. Dotted lines outline the parietal bones. (h) Transplantation of parietal bone without sutures from *Gli1-CE;R26-Tdtomato*^{fl} mice into nude mice (control). One month later, *Gli1+* cells in the bone marrow space (arrows) do not contribute to the formation of new periosteum, dura or osteocytes. (i) Visualization one month after transplantation of sagittal sutures or parietal bones without sutures (non-suture transplant) dissected from CAG-EGFP mice together with the intact periosteum and dura. Dotted lines outline the original size of the transplants. (j) Quantification of the fold change of the transplant surface area from (i). Values are plotted as mean ±SEM. The numbers indicate mean fold change. *Student's t-test* was performed, **, p=0.006, n=12 transplants. Scale bar in panel i, 1mm; other scale bars, 100 μm.

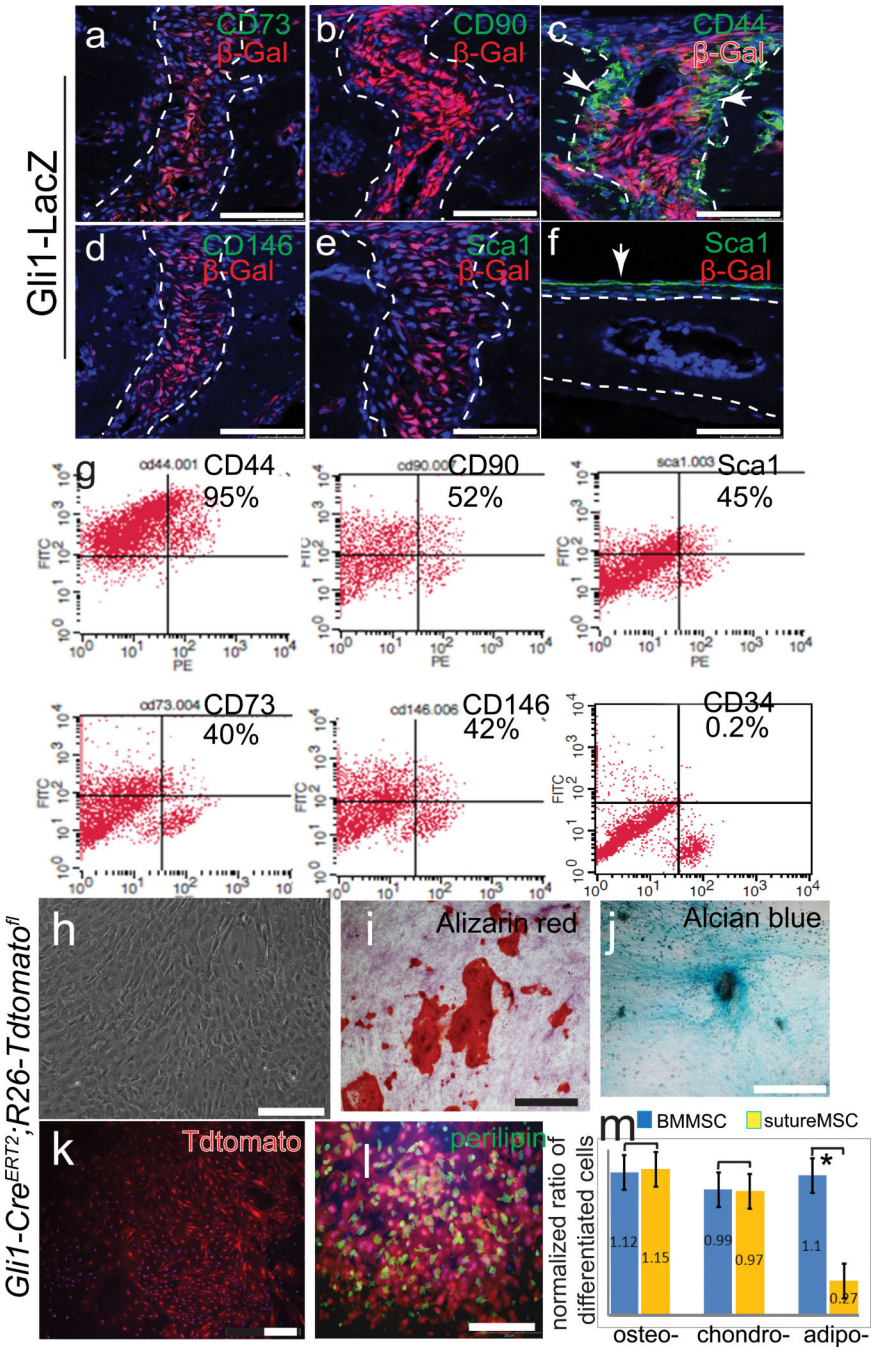

Figure 4.

Gli1+ cells are MSCs *in vitro*. (a-f) Immunohistochemical staining of MSC markers CD73 (a), CD90 (b), CD44 (c), CD146 (d) and Sca1 (e) in the suture mesenchyme of *Gli1-LacZ* mice. Sca1 expression is also detectable in the periosteum (f). Arrows indicate expression. Dotted lines outline bone margins. (g) FACS analysis of suture mesenchymal cells harvested from one-month-old *Gli1-CE;R26*^{Tdtomato} mice induced with tamoxifen. (h-l) *Gli1*+ cells form clones in culture. Positive clones were picked based on their fluorescence (k). Alizarin red (i), Alcian blue (j), and perilipin (l) staining indicates that cells from single clones can

undergo tri-lineage osteogenic (osteo), chondrogenic (chondro), and adipogenic (adipo) differentiation. (m) Quantitation of the fraction of differentiated cells in the suture MSC culture normalized to that of BMMSCs under the same conditions. Values are plotted as mean ±SEM. *, *student t-test*, p=0.02, n=5 cultures derived from different mice. Scale bars, 100 μm.

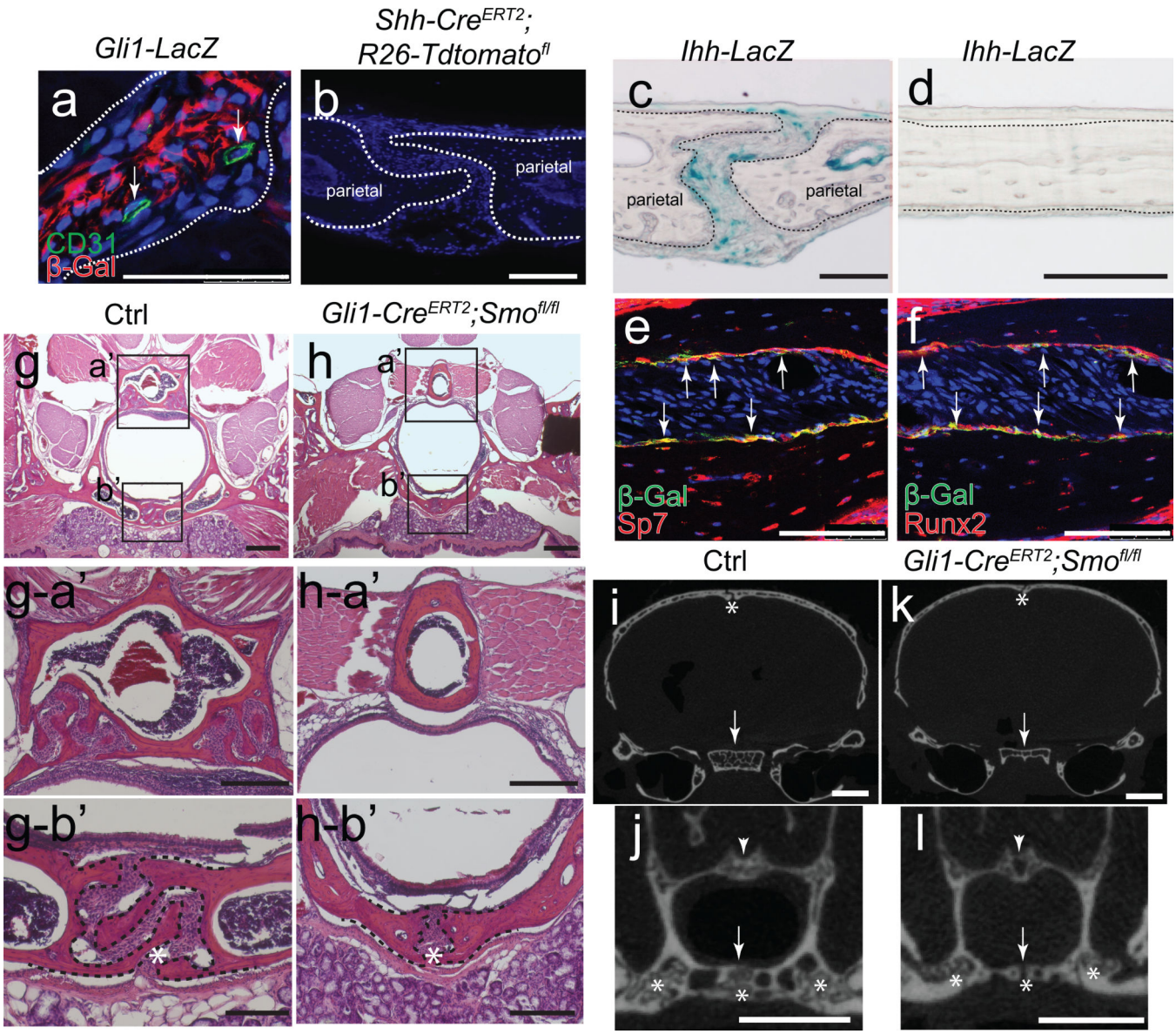

Figure 5.

IHH secreted from the osteogenic front signals to *Gli1+* cells in the suture mesenchyme and regulates osteogenic lineage differentiation. (a) Immunohistochemical staining of CD31 (green) in the sagittal suture in *Gli1-LacZ* mice. CD31 labels vasculature. Dotted line outlines the parietal bone. (b) Suture mesenchyme in *Shh-Cre^{ERT2};Tdtomato^{fl}* mice. One-month-old mice were induced and samples were collected two weeks later. (c,d) LacZ staining of the sagittal suture of *Ihh-LacZ* mice at 1 month of age. *Ihh+* cells are detectable at the osteogenic front of the parietal bone (c) but not in the periosteum or dura (d). Dotted line outlines the parietal bone margin. (e,f) Immunohistochemical staining (red) of Sp7 (e) and Runx2 (f) in the suture mesenchyme of one-month-old *Ihh-LacZ* mice. Yellow indicates colocalization of fluorescent staining (arrows). (g-l) HE staining (g,h) and microCT analysis (i-l) of one-month-old *Gli1-Cre^{ERT2};Smo$^{fl/fl}$* and *Gli1-Cre^{ERT2}* (ctrl) mice after induction with tamoxifen. Samples were collected 8 months later. Boxed areas in g and h are displayed

in the lower panels. MicroCT images in i and k are at the basosphenoid bone position. Arrows indicate basosphenoid bone; asterisks indicate patent sutures. MicroCT images in j and l are at the palatal bone position. Arrows indicate palatal bones; arrowheads indicate presphenoid bones; asterisks indicate patent sutures. Scale bars in panels i, j, k and l, 1mm; other scale bars, 100 μm.

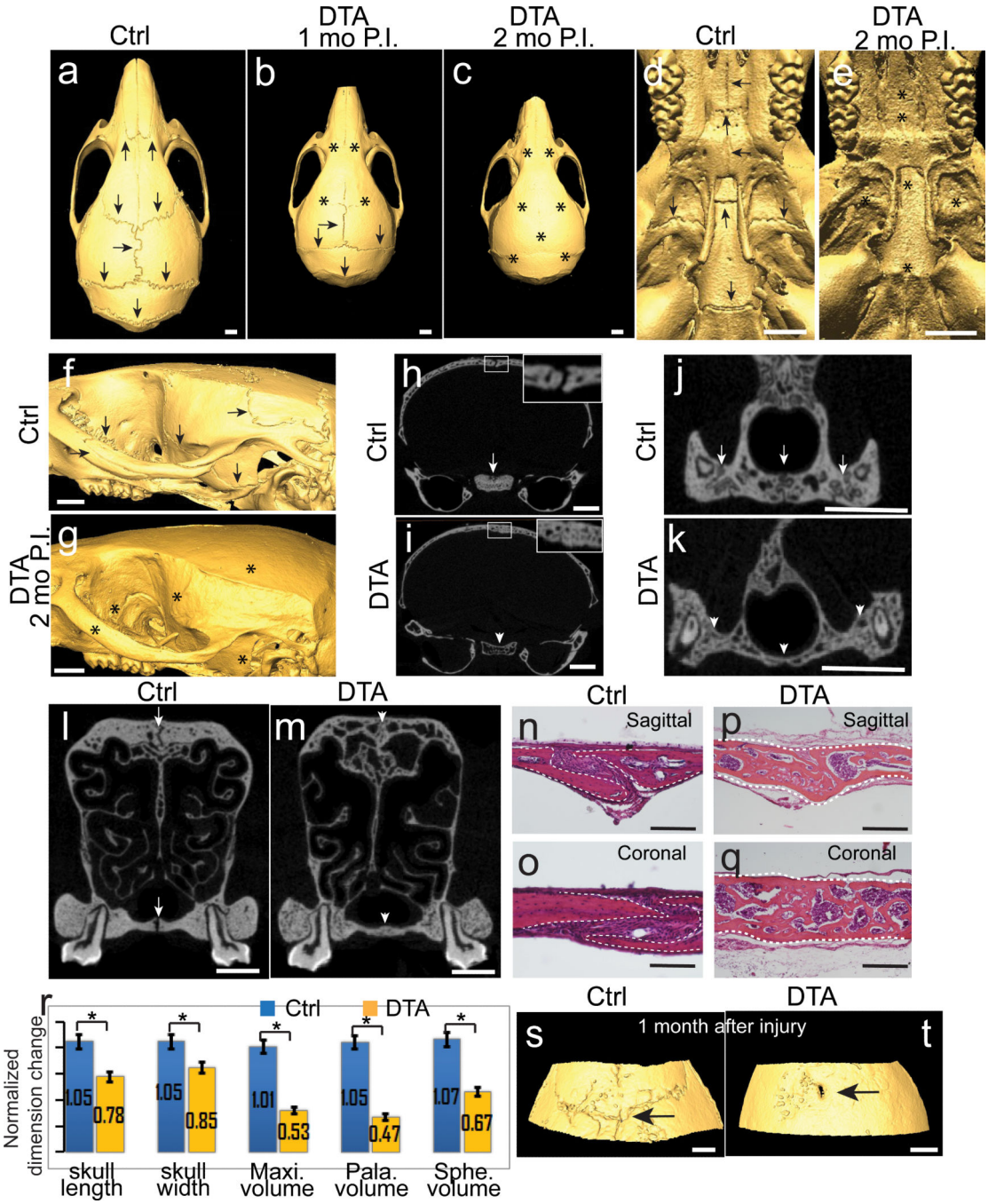

Figure 6.

Gli1+ cell ablation leads to craniosynostosis, skull growth arrest, osteoporosis and compromised injury repair. (a-g) Top views (a-c), bottom views (d,e) and side views (f,g) of microCT reconstructed images of *Gli1-CE* (Ctrl) and *Gli1-CE;R26*$^{DTAf/f}$ (DTA) mice induced with tamoxifen at one month of age. Samples were collected 1 month (b) or 2 months (c and all other panels) post-injection (P.I). Arrows indicate normal patent sutures. Asterisks indicate fused sutures in DTA samples. (h-i) MicroCT slices showing sagittal sutures in control and DTA mice. Basosphenoid bone in the DTA sample shows severe

osteoporosis (arrowhead) compared with the control (arrow). Boxed areas are displayed in the insets. (j-m) MicroCT images showing interpalatal and maxilla-palatal sutures (j,k) and frontal and intermaxillary sutures (l,m) from control and DTA mice. Arrows indicate patent sutures and arrowheads indicate fused sutures. (n-q) HE staining of sagittal and coronal sutures in control and DTA mice. Dotted lines outline margins of the bone. (r) Quantification of anterior-posterior skull length, left-right skull width, bone volume of the maxillary (maxi), palatal (pala) and basosphenoid (sphe) bone of control and DTA mice. Values are plotted as mean ±SEM. *, $p<0.05$. *Student t-test* analyses were performed to compare the skull length ($p=0.02$, n=5 skulls), skull width ($p=0.01$, n=5 skulls), maxillary bone volume ($p=0.02$, n=5 skulls), palatal bone volume ($p=0.02$, n=5 skulls) and sphenoid bone volume ($p=0.01$, n=5 skulls). (s, t) MicroCT images of one-month-old control and DTA mice injured five days after induction. Arrows in samples collected one month later indicate complete healing in the control sample and incomplete healing in the DTA sample. Scale bars in panels n-q, 200μm; other scale bars, 1mm.

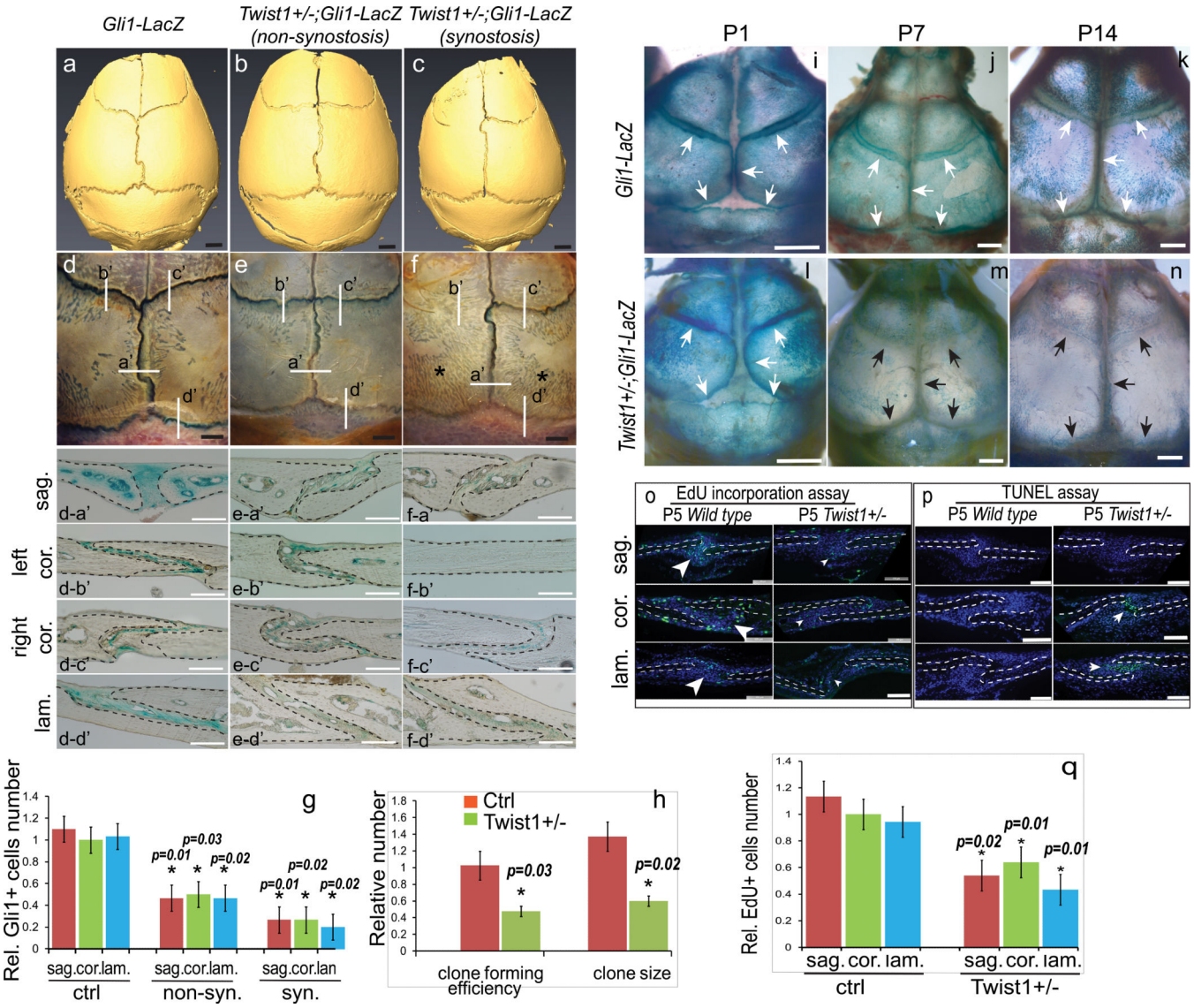

Figure 7.

Gli1+ cell numbers are significantly reduced in sutures of *Twist1*$^{+/-}$ mice. MicroCT (a-c) and whole mount LacZ staining (d-f) of one-month-old control Gli1-LacZ and *Twist1*$^{+/-}$*;Gli1-LacZ* $^{+/-}$ mice, with and without synostosis. Sagittal (sag), coronal (cor) and lamboid (lam) sections of each suture are displayed in the lower panels. White lines in d-f indicate the approximate positions of the sections. Dotted lines outline the margins of calvarial bones. Numbers of *Gli1*+ cells are quantified in (g). Values are plotted as mean ±SEM. *ANOVA* analysis was performed. *, p values are indicated in the figure, n=5 skulls. (h) Quantification of clone-forming efficiency and relative average clone size of sagittal suture mesenchymal cells from control (ctrl) and *Twist1*$^{+/-}$ mice. Values are plotted as mean ±SEM. *Student t-test* analysis was performed. *, p values are indicated in the figure, n=4 skulls. (i-n) LacZ staining of the calvarial bones of *Gli1-LacZ* and *Twist1*$^{+/-}$*;Gli1-LacZ* mice at P1, P7 and P14. White arrows indicate LacZ staining and black arrows indicate reduced or diminished LacZ staining. (o-p) Edu incorporation and TUNEL assays in sagittal

(sag), coronal (cor) and lambdoid (lam) sutures of control and *Twist1*$^{+/-}$ mice at P5. Dotted lines outline bone surface. Arrowheads indicate EdU+ cells or TUNEL+ apoptotic cells. EdU+ cell ratios are quantified in (q). Values are plotted as mean ±SEM. *Student t-test* analysis was performed. *, p values are indicated in the figure, n=6 skulls. Scale bars in panels a-f and i-n, 1mm; other scale bars, 100 μm.